Anthony Marin, Anthony Garcia, Ricardo Cruz* and Shashank Priya

High Efficiency Vibration Energy Harvesting Through Combined Isolator and Absorber Approach

DOI 10.1515/ehs-2016-0006

Abstract: Relative motion is required for vibration energy harvesting, such as magnet moving past the coil in inductive approach and tip-mass motion in piezoelectric approach. Typically, relative motion is created by amplifying the source displacement and storage of mechanical energy in an auxiliary vibrating mass. In this study, we propose a novel technique to create the relative motion without amplification of the original source displacement. The technique relies on cancelling the vibration at one location and transferring the source vibration directly to another location through combination of a vibration isolator with a vibration absorber. In this multi-degree of freedom configuration, the power is harvested from the displacement of the vibrating source rather than the displacement of an auxiliary mass. This configuration eliminates the need to capture relative motion with respect to an externally fixed component. A prototype was designed and fabricated based on this concept which was found to harvest 45 mW at 0.9 G base acceleration and weighed 462 g. Through analytical modeling it was determined that the prototype could generate 87 mW @ 1 G base acceleration, while weighing only 243 g. Also, an optimal balance between the bandwidth and the maximum power harvested was identified through parametric analysis.

Keywords: energy harvesting, multi-degree of freedom, relative displacement

Introduction

Vibration energy harvesting has been widely investigated in an effort to develop power source for the distributed wireless sensor nodes. The power requirement of various health and condition monitoring systems continues to decrease and thus many industries are exploring vibration energy harvesting to power the sensors in order to reduce the maintenance cost and improve the lifetime. At larger dimensions (>1 cm^3), induction based vibration energy harvesters are preferred and within this category there are two suitable mechanisms, namely four bar magnet configuration (El-hami et al. 2001; Glynne-Jones et al. 2004; Poulin, Sarraute, and Costa 2004; Stephen 2006; Beeby, Tudor, and White 2006; O'Donnell et al. 2007; Zhu et al. 2010) and magnetic levitation (Constantinou, Mellor, and Wilcox 2007; Saha et al. 2008; Mann and Sims 2009; Dallago, Marchesi, and Venchi 2010; Bonisoli et al. 2010; Galchev, Hanseup, and Najafi 2011). Our prior research on four bar magnet (Oliver and Priya 2009; Marin, Bressers, and Priya 2011) and magnetic levitation (Marin et al. 2011; Marin and Priya 2012) has focused on enhancing the electromagnetic coupling which is the factor correlating the conversion of mechanical to electrical energy.

Researchers have also started to consider alternatives to the four bar magnet and magnetic levitation prototypes to further improve the power density. In this aspect, efforts have been made to utilize the vibration absorbers as vibration attenuators and energy harvesters. Cornwell et al. have considered vibration absorbers for energy harvesting and developed the initial models (Cornwell et al. 2005). Other researchers have considered dynamic magnifiers, which are essentially vibration absorbers excited with base excitation rather than at the location where one is trying to eliminate the motion, with the intent to increase the bandwidth of harvesting (Lee, Youn, and Jung 2009; Chtiba et al. 2010; Ma, Kim, and Kim 2010; Aldraihem and Baz 2011; Arafa et al. 2011; Tang and Zuo 2011; Li, Liu, and Hsiao 2011; Zhou, Penamalli, and Zuo 2012).

In this study, we modeled and fabricated a multi-degree of freedom vibration energy harvester that cancels the vibration at one location and transfers the source vibration directly to another location through combination of a vibration isolator with a vibration absorber. In this novel configuration, the power was harvested from

***Corresponding author: Ricardo Cruz,** Center for Energy Harvesting Materials and Systems (CEHMS), Bio-Inspired Materials and Devices Laboratory (BMDL), Virginia Tech, Blacksburg, VA 24061, USA, E-mail: rcruzf@vt.edu

Anthony Marin, Anthony Garcia, Shashank Priya, Center for Energy Harvesting Materials and Systems (CEHMS), Bio-Inspired Materials and Devices Laboratory (BMDL), Virginia Tech, Blacksburg, VA 24061, USA

the displacement of the vibrating source mass rather than from the vibrating auxiliary mass allowing the system to harvest energy from relative motion between the source and primary mass within the device. Such configuration thus can harvest energy without the need of an externally fixed component, making the device easy to mount, as the utilized relative motion is captured from components within the device itself. Furthermore, as energy is harvested directly from the source displacement, one does not need amplification of the source vibration which could modify the system dynamics. Figure 1(a)–(c) schematically describe the novel proposed concept. Figure 1 (a) represents the spring-mass-damper model of a vibration isolator. In a vibration isolator, the damping constant c_i and spring constant k_i are designed to reduce the displacement transmissibility from the vibration source to the isolator mass m_i. This is achieved by choosing the isolator spring constant and mass which results in a natural frequency that is at least 1.4 times less than the frequency of the vibration source. Increasing the frequency ratio further and decreasing the damping allows for near cancellation of the isolator mass displacement. Figure 1(b) represents the vibration model of a vibration absorber. A vibration absorber consists of two spring-mass-damper systems where masses and springs are designed to protect the primary mass from vibrating while under an applied harmonic force F(t). The primary mass m_p and spring k_p and absorber mass m_a and spring k_a are designed such that their natural frequencies match. When choosing a ratio between the absorber and primary masses between 0.05 and 0.25, the energy supplied to the primary mass from the applied force is transferred to the absorber mass leading to large oscillations of the absorber mass. The presence of the damping eliminates the possibility of isolating the motion of the primary mass and therefore it is desirable to reduce the damping constants c_p and c_a.

There is a limitation in the performance of the vibration absorber, which is that the absorber spring stiffness must be able to withstand the full force of excitation and the deflection that results. Later in this paper, we will provide details on how this limitation affects the performance and how the electromechanical damping constant c_e limits the amount of power extracted from the system and the efficiency to 0.5. By combining the two systems (absorber and isolator) we propose to create relative motion between the moving vibration source and the almost stationary primary mass as shown in Figure 1(c).

Source displacements from real world applications are often on the level of 0.02–2 mm. This presents a challenge in harvesting the low displacement vibration. To this end, we can convert the linear vibration to rotational motion and amplify the rotational motion using a gear train. In this system (Figure 1(c)), a rack was connected to the vibration source and a gear train to the primary mass. When the vibration source was excited, it induced a force in the primary mass by the rack and pinion mechanism while displacement was absorbed by the auxiliary mass. In other words, a relative motion between the vibration source and almost-still primary mass was created.

Multi-degree of Freedom Harvester Design

Macro Scale Harvester Design

Initially, in order to validate the concept experimentally, a model 210 Rectilinear Control System manufactured

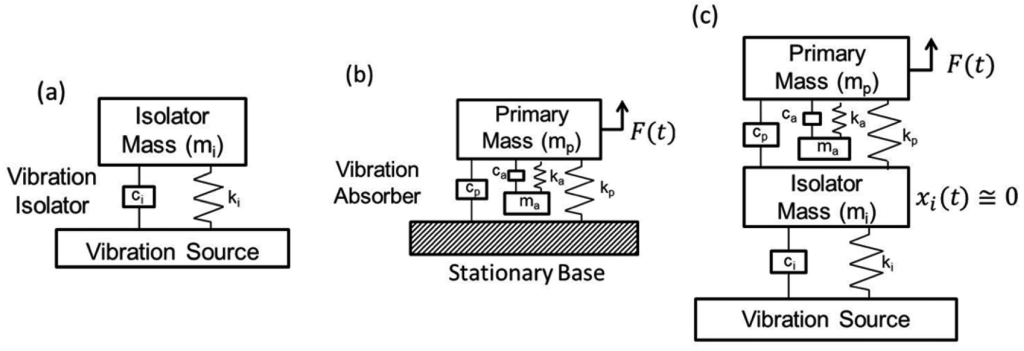

Figure 1: The multi-degree of freedom concept described through representative spring-mass-damper models. (a) Vibration isolator, (b) vibration absorber, (c) vibration isolator and absorber combined to create relative motion between the vibration source and almost stationary base.

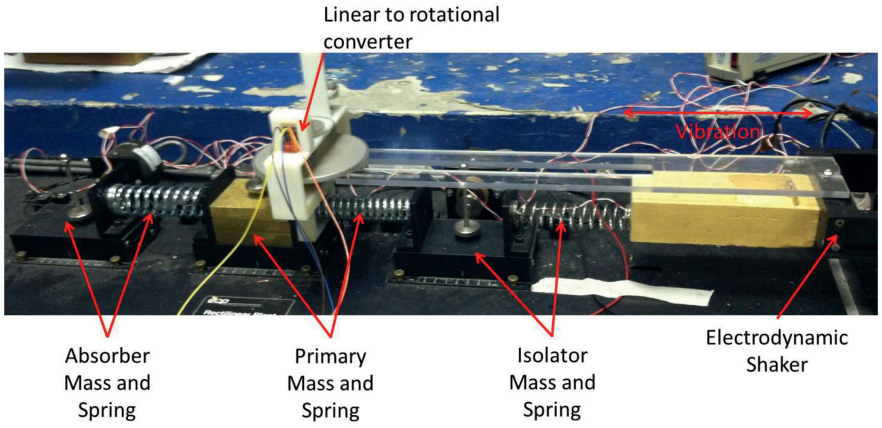

Figure 2: Setup of the macro scale multi-degree of freedom system.

by Education Control Products was modified to physically represent the spring mass damper, schematically shown in Figure 1(c). This prototype will be referred as the macro scale prototype in this paper and is shown in Figure 2. It should be noted that the system rests on the floor and therefore is not practical, though the setup provided a convenient way to confirm the concept and initial modeling approach. The system consisted of three carts which act as seismic masses (m_i, m_p, m_a).

The damping was from the kinetic friction within the linear slide bearings for each mass cart. The stiffness was provided by the steel mechanical compression springs. An electrodynamic shaker (APS 113) was attached to the isolator spring to represent the vibration source. The isolator component was designed to have a natural frequency of 4 Hz and the natural frequency of the primary and absorber mass components were 13 Hz. The values of the mass and spring constants for the experimental data shown later in the paper are listed in Table 1. The damping ratios are also listed in this table as provided by the manufacturer.

Table 1: Macro scale mechanical system parameters.

Component	Mass (kg)	Stiffness (N/m)	Damping ratio	Component natural frequency (Hz)
Isolator	0.59	390	0.04	4.09
Primary mass	2.82	18,843	0.04	13.01
Absorber mass	0.693	4,932	0.06	13.43

A linear to rotational converter, gear train and electromagnetic generator were attached to the primary mass in an effort to extract the electrical energy from the mechanical system. The relative motion between the shaker arm (base) and the primary mass will be used to rotate the primary shaft. Figure 3 shows the linear to rotational conversion mechanism which consisted of a pawl and ratchet. During oscillation, the relative motion between the base and primary mass allows the pawl to turn the ratchet transferring rotational motion to the primary shaft. Attached to the primary shaft was an encoder which was used to measure the angular displacement. A gear ratio of 1:10.83 was used to amplify the rotational velocity from the primary shaft to the secondary shaft. Attached to the secondary shaft was a permanent magnet generator that was used to convert the mechanical energy to electrical energy.

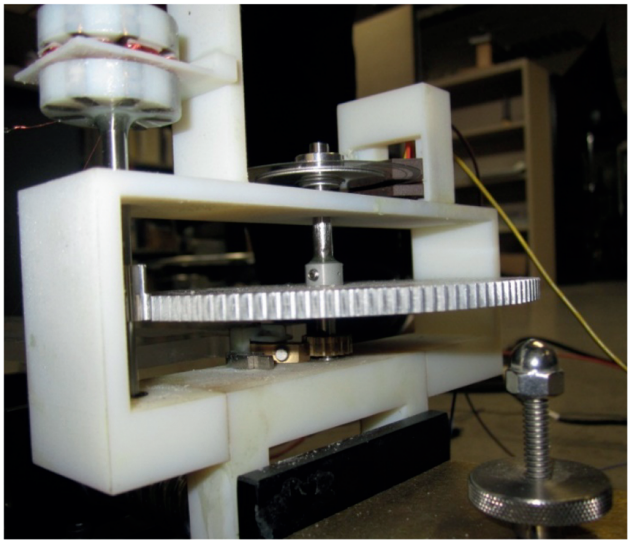

Figure 3: Linear to rotational gear train and generator.

Meso Scale Harvester Design

The macro scale prototype rested on the floor and therefore could not be applied in real world application. To this end, we designed a meso scale prototype which can be mounted on a vibrating source or electrodynamic shaker in lab as shown in Figure 4(a) and (b). The meso scale prototype consists of three masses which can vibrate freely along low friction linear rail bearings. The masses are connected by various steel springs to provide the required stiffness. The structure is mounted on an electrodynamic shaker (APS 113) which provides the source displacement as shown in Figure 4(a). The values for the mass and spring constants are listed in Table 2 below.

A linear to rotational converter, gear train, and electromagnetic generator assembly are attached to the primary mass as shown in Figure 4(b). The relative motion between the shaker arm (base) and primary mass was used to rotate the primary shaft. The linear to rotational motion converter consists of a rack and pinion in an effort to enhance the conversion efficiency. With a rack and pinion the force is transferred to the shaft in multiple directions and therefore rotates the shaft in two directions. This is undesirable as the generator would spin in one direction and then reverse preventing the ability to utilize the inertia of the generator. Therefore, a double clutch and differential was implemented to convert the oscillatory rotation to unidirectional rotation. Rather than designing a custom mechanism, Kobalt manufactured Double Drive screw driver that contains this mechanism was utilized. A similar mechanism was also custom designed for an energy harvester integrated in a suspension damper (Li et al. 2013). The rotational velocity was amplified using a planetary gear set which was purchased from Edmund Scientific. The planetary gear set can achieve gear ratios from 1:4 to 1:400.

Table 2: Meso scale mechanical system parameters.

Component	Mass (kg)	Stiffness (N/m)	Damping ratio	Component natural frequency (Hz)
Isolator	0.083	42	Unknown	3.58
Primary mass	0.3	2,189	Unknown	13.6
Absorber mass	0.079	618	Unknown	14.04

Attached to the secondary shaft was a permanent magnet generator used to convert the mechanical energy to electrical energy. The axial permanent magnet generator consisted of a rotor that housed eight rectangular magnets arranged in a circular array with adjacent magnets having alternate polarity, and a stator of eight tear drop shape coils winded with 42 AWG magnet wire. The resistance of the generator was 1,964 Ω and the generator constant was 15.33 V*s/m.

Analytical Modeling and Theoretical Analysis

To model the dynamics of the multi-degree of freedom harvester a spring-mass-damper approach was used. The equation of motion for the isolator under constant displacement from a vibration source consisted of:

$$m_i\ddot{x}_i + c_i(\dot{x}_i - \dot{x}_s) + k_i(x_i - x_s) + c_p(\dot{x}_i - \dot{x}_p) + k_p(x_i - x_p) = 0 \quad [1]$$

where m_i is the isolator mass, c_i and c_p are the isolator and primary mass damping constants, k_i and k_p are the isolator and primary mass spring constants, $x_s, x_i,$ *and* x_p

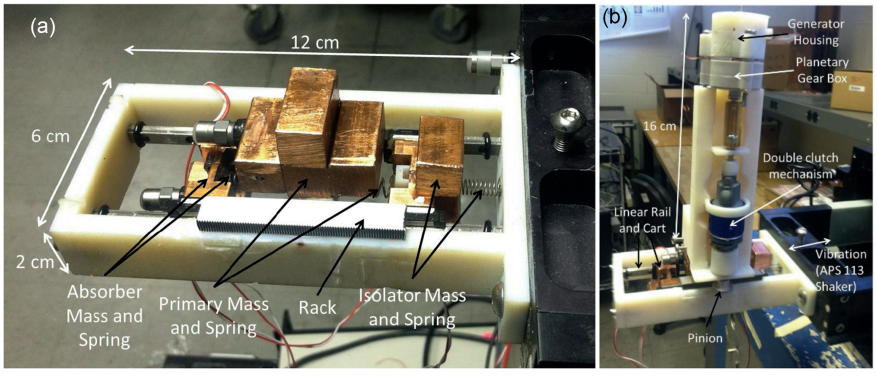

Figure 4: Image of meso scale harvester (a) close-up of combined isolator and absorber system (b) close-up of linear to rotational converter, gear train, and generator.

are the displacements of the source mass, isolator mass, and primary mass, and ω_s is the source vibration frequency. Equation [1] can be re-arranged to a more convenient form with a denoting source displacement and expressed as:

$$m_i\ddot{x}_i + (c_i + c_p)\dot{x}_i + (k_i + k_p)x_i - c_p\dot{x}_p - k_p x_p = c_i a\omega_s \cos\omega_s t + k_i a \sin\omega_s t \quad [2]$$

The equation of motion for the primary absorber mass with applied force from the vibrating source consisted of:

$$m_p\ddot{x}_p + c_p(\dot{x}_p - \dot{x}_i) + k_p(x_p - x_i) + c_a(\dot{x}_p - \dot{x}_a) + k_a(x_p - x_a) = F_s \sin\omega_s t \quad [3]$$

where m_p is the primary mass and F_s is the force applied to primary mass from source. Equation [3] can be rewritten in a more convenient form and expressed as:

$$m_p\ddot{x}_p + (c_p + c_a)\dot{x}_p - c_p\dot{x}_i - c_a\dot{x}_a + (k_p + k_a)x_p - k_p x_i - k_a x_a = F_s \sin\omega_s t \quad [4]$$

The equation for the motion of the secondary absorber mass was:

$$m_a\ddot{x}_a + c_a(\dot{x}_a - \dot{x}_p) + k_a(x_a - x_p) = 0 \quad [5]$$

The coupled equations of motion were separated into mass, damping and stiffness matrices to be solved using MATLAB both analytically and numerically. The analysis was utilized to design the two different size scale harvesters introduced above. To first determine if the relative motion between the harvester base and primary mass could be created through combination of isolator and absorber, the dynamics of the system were simulated without the electromechanical coupling term which will be added later in the analysis. By performing a modal analysis of the undamped three degree of freedom system, the natural frequencies and the corresponding mode shapes of the macro and meso scale systems were calculated in order to better understand the system dynamics, shown in Tables 3 and 4.

Table 3: Macro scale modal analysis.

		Macro scale		
Natural frequencies, ω (*Hz*)		1.5383	14.6816	31.6487
Mode Shape	$\begin{bmatrix} M_i \\ M_p \\ M_a \end{bmatrix}$	$\begin{bmatrix} -0.4853 \\ -0.4938 \\ -0.5004 \end{bmatrix}$	$\begin{bmatrix} -0.2830 \\ -0.2134 \\ 1.0906 \end{bmatrix}$	$\begin{bmatrix} -1.1745 \\ 0.2554 \\ -0.0561 \end{bmatrix}$

Table 4: Meso scale modal analysis.

		Meso scale		
Natural frequencies, ω (*Hz*)		1.5706	14.2738	29.4987
Mode shape	$\begin{bmatrix} M_i \\ M_p \\ M_a \end{bmatrix}$	$\begin{bmatrix} -1.5122 \\ -1.5357 \\ -1.5565 \end{bmatrix}$	$\begin{bmatrix} -0.6670 \\ -0.4764 \\ 4.5944 \end{bmatrix}$	$\begin{bmatrix} -3.0523 \\ 0.8649 \\ -0.2329 \end{bmatrix}$

The analytical frequency responses of the undamped macro and meso scale devices can be seen in Figure 5. These frequency responses are consistent with the frequencies and mode shades calculated.

The mode shape of interest would be the one that achieves the desirable relative motion between the primary mass and the vibrating source. This can be achieved by isolating the isolator mass and transferring most of the force from the source, through the primary mass, to the absorber mass. For both cases this mode shape is found at the second natural frequencies, being 14.68 Hz for the macro scale system and 14.27 Hz meso scale system. From these simulations of an analytical undamped three degree of freedom system model, we expect that

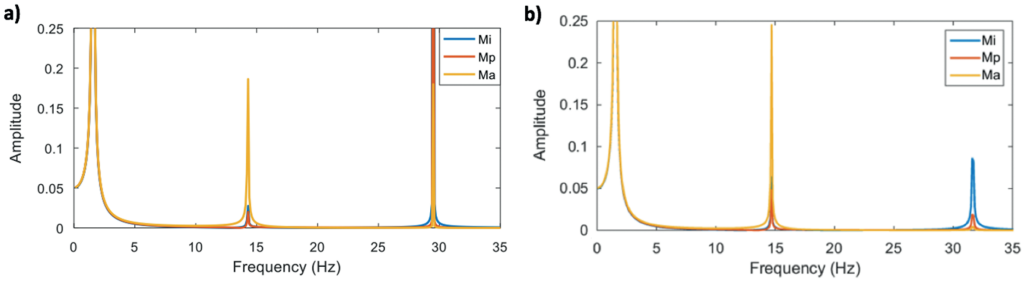

Figure 5: Frequency responses for (a) marco scale system and (b) meso scale system.

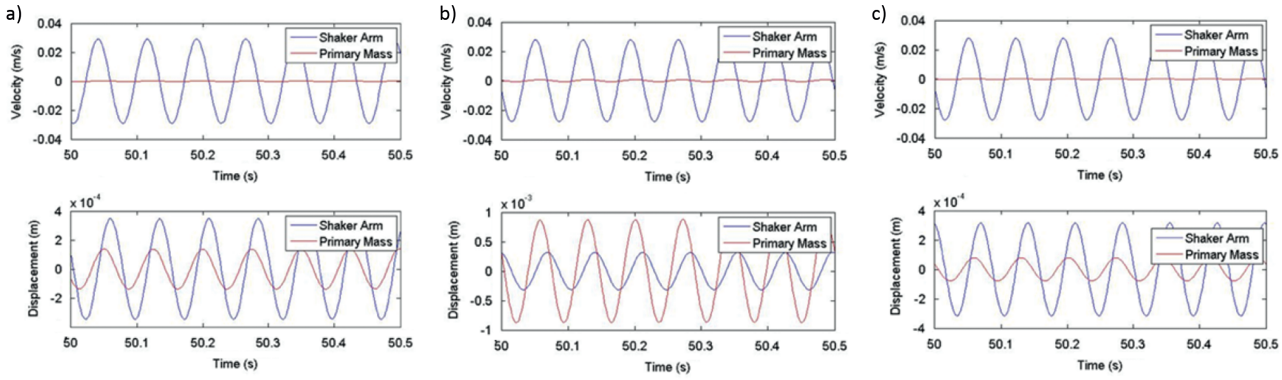

Figure 6: Dynamic simulation of (a) macro scale prototype in response to base excitation of 0.25 G and 13.4 Hz (b) meso scale prototype in response to base excitation of 0.25 G and 14 Hz with larger shaker (c) meso scale prototype in response to base excitation of 0.25 G and 14 Hz with smaller shaker.

relative motion can be achieved by using an isolator and absorber configuration to harvest energy.

A numerical simulation of the three degree of freedom system was also performed, Figure 6(a)–(c) displays the time response results of the dynamic simulation for the macro and meso scale prototypes under a base excitation of 0.25 G. The force of the source was calculated using the mass of the shaker arm which was 2.3 kg for the APS 113. The macro scale prototype was excited at 13.4 Hz which leads to a base velocity and base displacement of 29.2 mm/s and 0.347 mm at 0.25 G. For the macro scale prototype, motion is essentially canceled at the primary mass and 29.1 mm/s and 0.272 mm of relative motion existed. The meso scale prototype was excited at 14 Hz which leads to a base velocity and base displacement of 27.8 mm/s and 0.316 mm at 0.25 G. For the meso scale prototype under the same base excitation as the macro scale prototype, 27.3 mm/s and 0.739 mm of relative motion existed. As shown in Figure 6(a) and (b), unlike the macro scale prototype, the meso scale prototype was not cancelling the motion of the primary mass. It is clear from the plot of displacement in Figure 6(b) that the primary mass is moving more than the shaker arm suggesting that absorber is unable to transfer the force. The absorber spring in the macro scale prototype is 8 times stiffer than the meso scale prototype. Therefore, the meso scale shaker arm mass had to be changed in order to achieve isolation in the primary mass. As shown in eq. [4], the force of the shaker will be directly related to the vibrations of our system. As a result, the meso scale system was then simulated with a 0.25 G base excitation from a smaller shaker with moving a mass of only 0.2 kg and the results are shown in Figure 6(c). When the cancellation was achieved, 27.8 mm/s and 0.273 mm of relative motion existed. These simulations prove the existence of relative motion between the shaker arm and primary mass with the combination of a vibration isolator and absorber.

The simulation results in Figure 6(a) did not include any conversion from mechanical to electrical energy as we did not include the electromechanical coupling term. In order to add the coupling term, we have to modify eq. [4]. The dynamic model assumes that all the applied force from the source is transferred to the primary mass and then to the absorber mass. When we attach a linear to rotational converter to the primary mass, the force applied from the shaker arm does not transfer directly to the primary mass due to the moment arm of the pinion. When we place an electrical load on the generator the backward coupling torque is applied to the shaft and due to the moment arm of the pinion a force is applied to the primary mass. In our modeling approach, we assume that the force from the source can overcome any electrical load that we place on the system. To derive the backward coupling force at the rotational generator we start with the force on a moving conductor in a magnetic field which consists of:

$$\vec{F} = I\vec{L} \times \vec{B} \qquad [6]$$

According to the above equation the force is solely dependent upon the magnitude of current flow since the coil length L and magnetic flux density B remain constant in the rotational generator. If the velocity vector is perpendicular to the magnetic flux vector the magnitude of current flow can be determined by eq. [7]:

$$I(t) = \frac{B(t)Lv}{(R_c + R_L)} \quad [7]$$

From eq. [7], the current is solely dependent upon the magnetic flux density $B(t)$ as the coil resistance R_c, load resistance R_L, velocity v, and coil length L are all constant in the rotational generator. For the rest of the analysis, we replace $B(t)L$ with Φ(t) which provides a more accurate representation of the electromagnetic coupling term (Marin, Bressers, and Priya 2011). The force can be derived by the following relationship:

$$F(t) = \Phi(t)I(t) = \Phi(t)\frac{(\Phi(t)v)}{(R_c + R_{L)}} = \frac{(\Phi(t))^2}{(R_c + R_L)}v \quad [8]$$

Equation [8] contains a coupling term which varies with time. Through simulation we predict the maximum Φ and divide by $\sqrt{2}$ as the variation of $\Phi(t)$ is sinusoidal. Therefore, the average generator torque in terms of angular velocity can be derived by the following relationship:

$$\tau_{generator,\,avg} = F_{avg}r_{gen} = \frac{\Phi_{max}}{\sqrt{2}}I(t)r_{gen} = \Phi_{max}\frac{\Phi_{max}}{2(R_c + R_L)}r_{gen}{}^2\dot{\theta} = \frac{(\Phi_{max})^2 r_{gen}{}^2}{2(R_c + R_L)}\dot{\theta} \quad [9]$$

where r_{gen} is the radius of the generator which was 10 mm. To relate the torque at the generator to a force at the pinion which translates to a damping force applied to the primary mass we set torque at the pinion equal to the torque at the generator and derive the electrical damping constant c_e; as a result, the torque at the pinion can be written as:

$$\tau_{pinion} = c_e\left(\dot{x}_p - \dot{x}_s\right)r_{pin} \quad [10]$$

where

$$\dot{x}_s = x_s\omega_s\cos\omega_s t \quad [11]$$

where r_{pin} is the radius of the pin which was 6.5 mm. In eq. [10], the relative velocity varies in sinusoidal fashion with time. The relative velocity in eq. [9] is a constant. In order to relate the relative velocity to a constant angular velocity, the maximum value of the relative velocity divided by the $\sqrt{2}$ for one period during steady state was used for the approximating the angular velocity of the pinion. Setting the $\tau_{generator} = \tau_{pinion}$ and solving for c_e leads to the following relationship where N is the gear ratio:

$$c_e = \frac{N^2(\Phi)^2 r_{gen}{}^2}{2r_{pin}{}^2(R_c + R_L)} \quad [12]$$

The equation of motion for the primary absorber mass with the electromechanical coupling term included now consists of:

$$m_p\ddot{x}_p + \left(c_p + c_a + c_e\right)\dot{x}_p - c_p\dot{x}_i - c_a\dot{x}_a + \left(k_p + k_a\right)x_p - k_p x_i - k_a x_a = c_e x_s\omega_s cos\omega_s t \quad [13]$$

Kirchhoff's voltage law was applied in eqs. [14]–[17] to compute the maximum steady state voltage and steady state power.

$$0 = \Phi(t)r_{gen}\dot{\theta}_{gen} - R_c i(t) - R_L i(t) \quad [14]$$

$$i(t) = \frac{\Phi(t)r_{gen}\dot{\theta}_{gen}}{R_c + R_L} \quad [15]$$

$$P = i(t)^2 R_L = \frac{\Phi(t)^2 r_{gen}{}^2\dot{\theta}_{gen}{}^2}{(R_e + R_L)^2}R_L \quad [16]$$

$$P_{avg} = \frac{1}{2}\frac{\Phi_{max}{}^2 r_{gen}{}^2\dot{\theta}_{gen}{}^2}{(R_e + R_L)^2}R_L \quad [17]$$

To investigate the scaling relationship of the energy harvester we varied the gear ratio which varies the magnitude of the electromechanical coupling term c_e to determine the optimum gear ratio for a variety of different isolator, primary, absorber mass values. While the primary and absorber mass values were varied the spring constants were varied accordingly so the component natural frequency was 13.6 Hz for all combinations. The performance of each configuration was compared in terms of power output normalized by total mass. A base excitation of 1 G and a linear to rotational conversion efficiency of 62% was used for the parametric analysis. Figure 7(a)–(d) displays the results of the analysis. In Figure 7(a), 14 different configurations of primary and absorber masses for two isolator mass values are compared to determine if the mass of the isolator affects the power output. From Figure 7(a), it was determined that there was no correlation between the normalized power output and isolator mass. Therefore, for the rest of the analysis only the 14 primary/absorber mass combinations are analyzed. Figure 7(b) analyzes the effect of the absorber/primary mass ratio on normalized power output. From the analysis a linear and direct relationship between the mass ratio and power output was found to exist. The result was somewhat unexpected as it is typical for a well-designed absorber mass ratio to be between 0.05 and

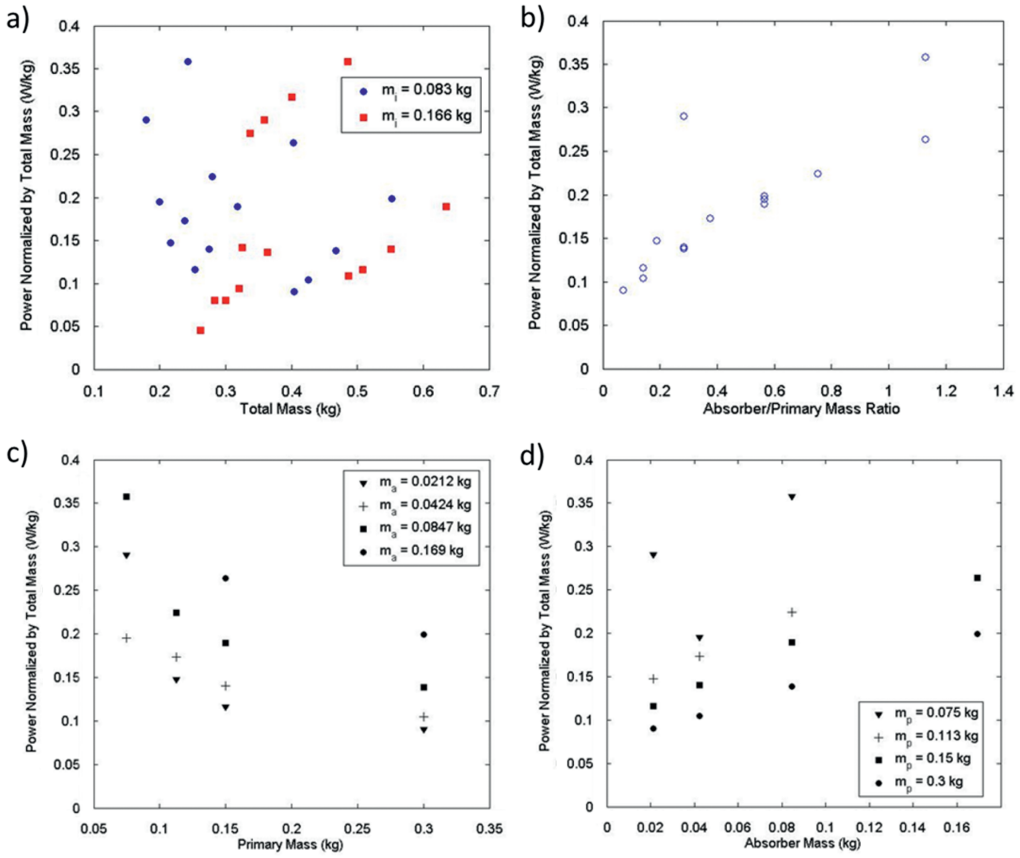

Figure 7: (a) Primary and absorber masses for two isolator mass values are compared to determine if the mass of the isolator affects the power output, (b) analysis of the effect of the absorber/primary mass ratio on normalized power output, (c) power output normalized by mass seems to increase with the decrease in primary mass squared, (d) power output normalized by mass is linearly and directly dependent on the absorber mass.

0.25 (Rahimi et al. 2012). To investigate the effect further, we analyzed the dependence of the magnitude of both the primary mass and absorber mass on the power output. The results of the analysis are shown in Figure 7(c) and (d) clearly illustrating the effect. Power output normalized by the mass is linearly and directly dependent on the absorber mass for every value of the primary mass as seen in Figure 7(d). The primary mass has a different effect; power output normalized by the mass seems to increase with the decrease in primary mass squared as seen in Figure 7(c). The result is unexpected as an absorber should perform worse and therefore decrease the relative motion between the base and the primary mass.

To further investigate the model, we evaluated the dynamic response for a frequency sweep from 1 to 20 Hz. Figure 8(a)–(d) displays the results of the analysis grouped by a range of mass ratios (0–1.13 kg). The results shown in Figure 8(a) and (b) are what one would expect for the frequency response of an absorber with a natural frequency of 13.6 Hz canceling the motion effectively; as a result, increasing the power output. Analyzing the results with mass ratios higher than 0.5 in Figure 8(c) and (d) shows that response is similar to what one would expect for a resonant system.

Experimental Results

Macro Scale Harvester

Performance of Isolator and Absorber Combination

To characterize the performance of the isolator and absorber combination, we evaluated (1) the magnitude of vibration for which isolator and absorber combination reduces the vibration at the primary mass, (2) if the force applied to the primary mass from the shaker arm

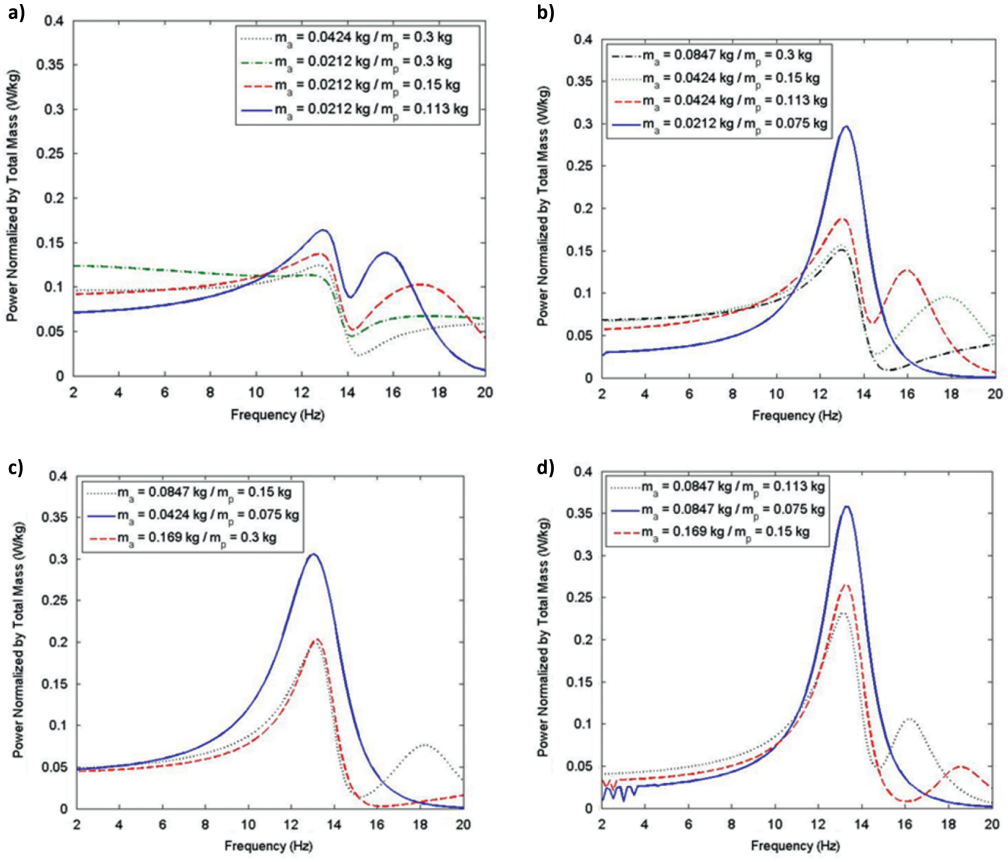

Figure 8: (a) Frequency response of systems with mass ratio of 0–0.25 kg, (b) 0.25–0.5 kg, (c) 0.5–0.75 kg, (d) 0.75–1.13 kg.

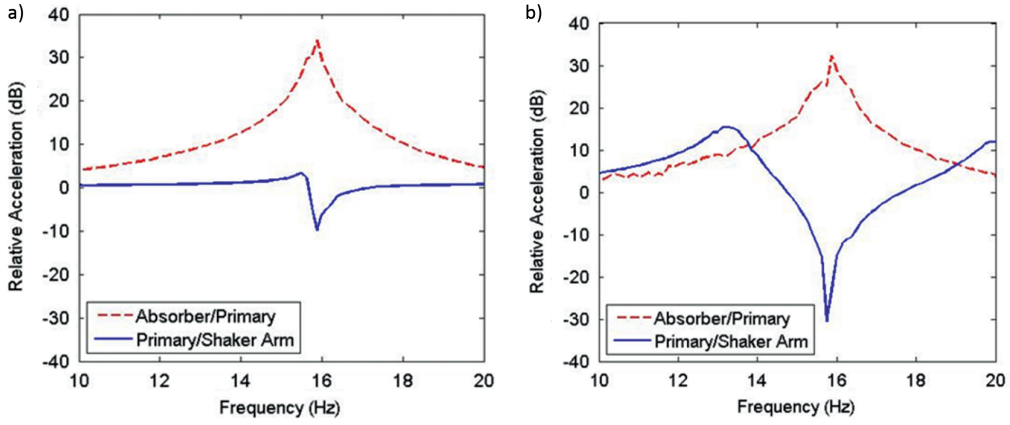

Figure 9: (a) Transfer function analysis for system with rigid connection, (b) transfer function analysis for system with semi rigid connection.

can be transferred to the absorber mass, and (3) the magnitude of relative motion created between the shaker arm and primary mass. In order to evaluate these questions, vibration frequency sweeps were applied to the macro scale system from 10 Hz to 20 Hz as the undamped simulation indicated that the desired mode shape would occur at a frequency of 14.68 Hz. Accelerometers were placed on the shaker arm and on each mass (isolator, primary, and absorber). Figure 9(a) and (b) displays the transfer functions between the primary mass and the shaker arm and between the absorber mass and the primary mass for two different operating conditions: (a) rigid connection was placed between the shaker arm and primary mass, and (b) semi-rigid connection between the shaker arm and primary mass. When the rigid connection was attached, the condition represented the maximum

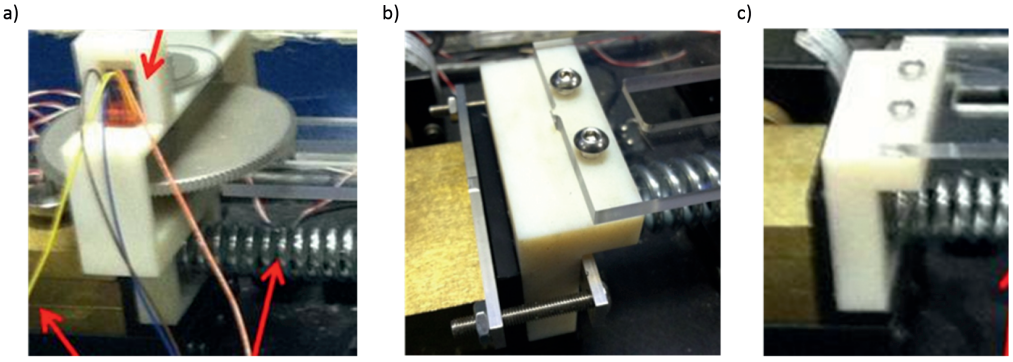

Figure 10: Images of the various connections used in the analysis (a) linear to rotational coupler (b) rigid connection, (c) semi-rigid connection.

force transfer condition as little or no relative motion should exist between the primary mass and shaker arm as shown in Figure 9(a). Although Figure 9(a) shows that at 15.8 Hz some relative motion existed due to the cancelation of the vibration at the primary mass location. Even though a rigid connection was used, the acrylic connector shown in Figure 3(a) bends resulting in a small relative motion. To determine how much relative motion existed with the applied force from the shaker, a semi-rigid connection was applied to the system. In this condition, in addition to the flexing of the acrylic connector, the ABS plastic primary mass connector can also flex. Figure 9(b) displays the relative acceleration between the primary mass and the shaker arm at 15.8 Hz. With a base acceleration of 0.28 G or 2.7 m/s^2, a relative acceleration of 2.2 m/s^2 was achieved. Acceleration higher than 0.28 G would cause the absorber spring to detach from its connector to the absorber mass due to the severity of the vibration magnitude. The experimental results further confirm the theoretical predictions that we can cancel the vibration at one location in order to create relative motion to harvest energy from the vibration source. The various connections and also linear to rotational motion converter are shown in Figure 10(a)–(c).

Energy Harvesting Capability and Performance

To determine the energy harvesting capability, electrical loads were placed at the output of the permanent magnet generator. The macro scale energy harvester was tested at four different base acceleration values of 1.07 G_{rms}, 1.24 G_{rms}, 1.41 G_{rms} and 1.76 G_{rms}. The steady state velocities of the primary shaft were measured in both open circuit and closed circuit condition with various resistances to determine the electrodynamic effect on the system as shown in Figure 11(a). As the load resistance is decreased towards short circuit condition, the electrodynamic force due to current flowing in the generator decreases the steady state angular velocity demonstrating that we are extracting electrical energy out of the system. Figure 11(b) displays the power as a function of load resistance at each base acceleration level. An optimum load resistance leads to maximum power extraction exists for each acceleration

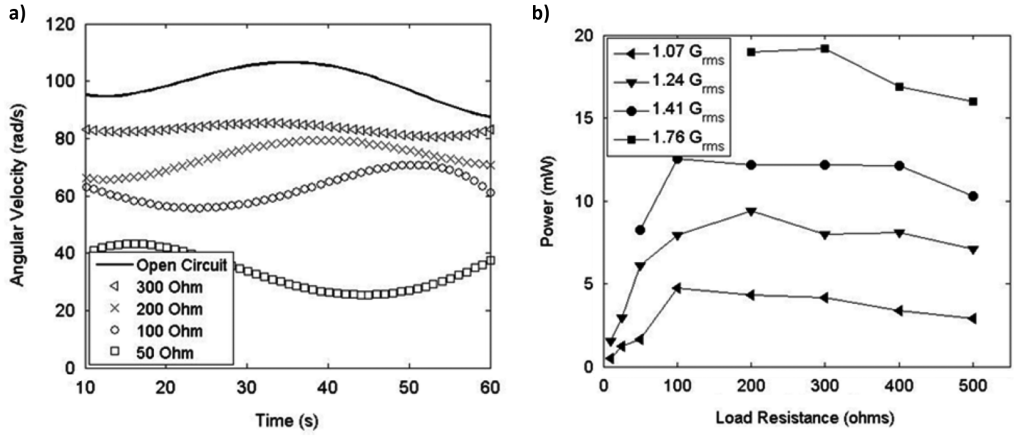

Figure 11: (a) Rotational velocity of primary shaft as a function of resistive load (b) power as a function of base acceleration.

value. This optimum load resistance increases in value as the base acceleration is increased.

Meso Scale Harvester

Isolator and Absorber Performance

To characterize the performance of the isolator and absorber combination for the meso scale prototype, we evaluated (1) the magnitude of vibration at which isolator and absorber combination reduces the vibration at the primary mass (2) if force applied to the primary mass from the shaker arm can be transferred to the absorber mass and (3) the magnitude of relative motion created between the shaker arm and primary mass. In order to evaluate these conditions vibration frequency sweeps were applied from 10 Hz to 20 Hz as the undamped simulation indicated that the desired mode shape would occur at a frequency of 14.27 Hz. Accelerometers were placed on the shaker arm and on each mass (isolator, primary, and absorber). Figure 12(a)–(c) displays the transfer functions between the primary mass and the shaker arm and between the absorber mass and the primary mass for three different operating conditions: (a) rigid connection was placed between the shaker arm and primary mass, (b) semi-rigid connection between the shaker arm and primary mass and (c) the linear to rotational converter between the shaker arm and the primary mass. The shaker used for the experimentation was a model TJ-5 from TmcSolution, rather than the APS 113 due to the effective moving mass (shaker arm) being 0.2 kg rather than 2.3 kg. The theoretical modeling showed that cancellation of the primary mass was only achievable with the smaller shaker (eq. [4]). When the rigid connection is attached as shown in Figure 13(a), the condition represents the maximum force transfer condition as little or no relative motion should exist between primary mass and shaker arm, as shown in Figure 12(a). Unlike the macro scale prototype, no relative motion was measured between the shaker arm and primary mass. The primary mass actually moved slightly more than the shaker arm. The amplitude of the absorber mass was highly damped as compared to the macro prototype suggesting that the linear rail bearings have higher friction as compared to the bearings on the macro scale system. To determine if relative motion existed with the applied force from the shaker, a semi rigid connection was applied to the system shown in Figure 13(b). In this condition, the ABS plastic connector is bowed to allow for more flexing during vibration. Limited relative motion is absorbed, however not significantly more compared to the rigid connection. Another experiment was conducted which consisted of connecting the primary mass and harvester base (shaker arm) with a rack and pinion which also acts as the linear to

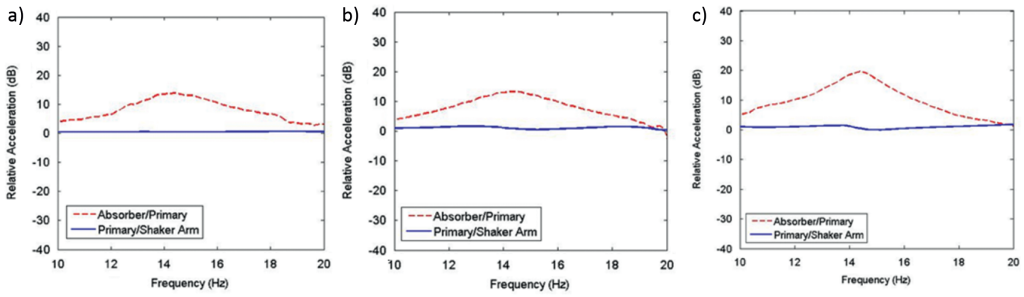

Figure 12: (a) Transfer function analysis for system with rigid connection, (b) transfer function analysis for system with semi rigid connection, (c) transfer function analysis for system with linear to rotational converter connected.

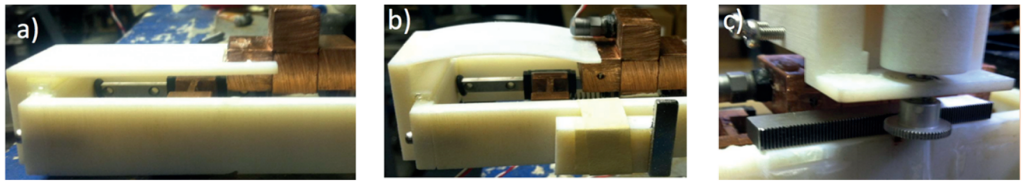

Figure 13: Images of the various connections used in the analysis (a) rigid connection, (b) semi-rigid connection, and (c) linear to rotational coupler (rack and pinion).

rotational coupler. The generator was loaded with a very high gear ratio in order to prevent substantial motion. In this condition, the primary mass is able to move slightly with an applied force from the shaker, similar to the condition that would be true during operation. This type of configuration was not tested on the macro scale prototype. Figure 12(c) displays the relative acceleration between the primary mass and the shaker arm at the operation frequency of 14.25 Hz. While the relative motion was much smaller than the macro scale prototype, we have confirmed the theoretical predictions with experimental results showing that we can cancel the vibration at one location to create relative motion to harvest energy from the source of vibration.

Energy Harvesting Capability and Performance

To determine the capability of the energy harvester, electrical loads were placed on the output of the permanent magnet generator. The gear ratio from the primary shaft to the generator shaft was 25:1. The meso scale energy harvester was tested at three different base acceleration values of 0.35 G_{rms}, 0.5 G_{rms} and 0.65 G_{rms} at a frequency of 14 Hz. The steady state velocities of the generator shaft are measured in both open circuit and closed circuit with various resistances to determine the electrodynamic effect on the system, as shown in Figure 14(a). As the load resistance is decreased towards short circuit condition the electrodynamic force due to current flowing in the generator decreases the steady state angular velocity suggesting we are extracting electrical energy out of the system. Figure 14(b) displays the power as a function of load resistance at each base acceleration level. An optimum load resistance which leads to maximum power extraction exists for each acceleration value. This optimum load resistance decreases in value as the base acceleration is increased. Next we present the result that shows that electrical energy can be extracted from this relative motion to realize the multi-degree of freedom vibration energy harvester concept.

To validate the theoretical modeling, a comparative analysis with the experiments was conducted. Figure 15 displays the results of the simulation with mass values of the prototype. The shape of the experimental trend of optimum load resistance vs power is shown in Figure 14 (b) matches well with the theoretical predictions shown in Figure 15; although the theoretical predictions over predict the power output. This is due to the simulations assuming 100 % linear to rotational energy conversion efficiency. For the analysis in the theoretical section

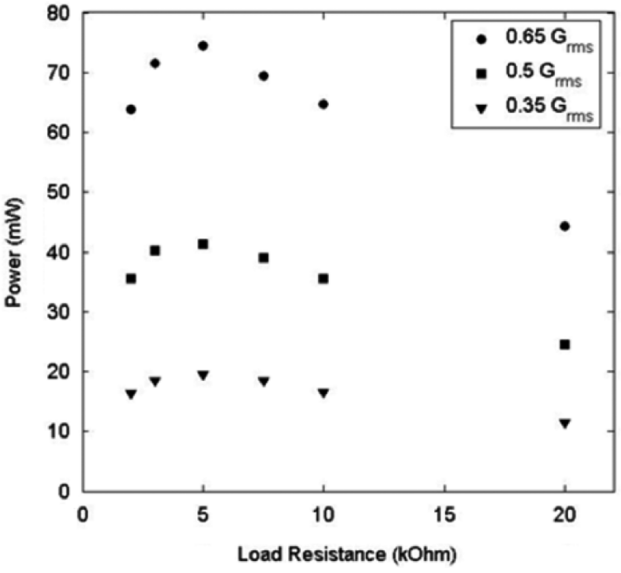

Figure 15: Load resistance vs. power as simulated by the model presented in the modeling section for gear ratio of 25:1.

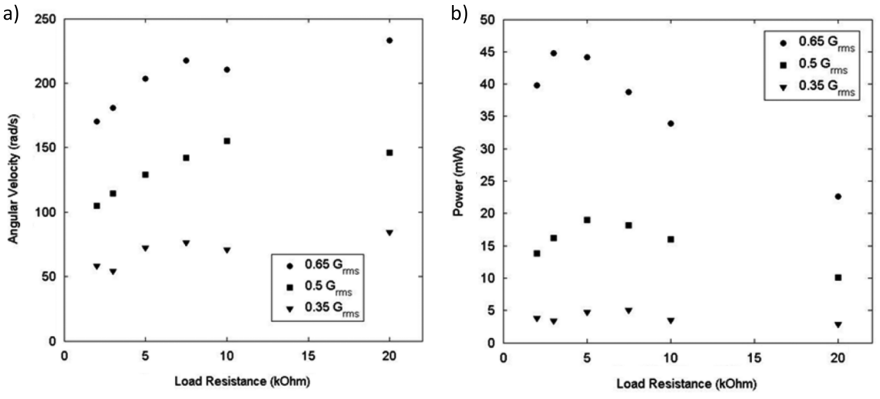

Figure 14: (a) Rotational velocity of primary shaft as a function of resistive load (b) power as a function of base acceleration.

Table 5: Values used to calculate the generator, linear-to-rotational and overall efficiencies.

AVG base acceleration (m/s^2)	6.79	6.86	6.79	6.65	6.58	6.51	6.38
AVG base velocity (m/s)	0.0772	0.0780	0.0772	0.0756	0.0748	0.0741	0.0725
AVG base power (W)	0.105	0.107	0.105	0.101	0.099	0.096	0.092
Generator angular velocity (RPM)	2,325	2,125	2,025	1,850	1,765	1,663	1,488
Max transformation factor (V*s/m)	15.39	15.27	15.01	15.40	15.18	15.20	15.83
Load resistance (ohm)	2,0000	10,000	7,500	5,000	4,000	3,000	2,000
Generator torque (mN*m)	0.131	0.217	0.253	0.330	0.357	0.405	0.493
Generator voltage (volts)	24.13	20.08	17.84	15.15	13.31	11.31	8.80
Generator power (W)	0.029	0.040	0.042	0.046	0.044	0.043	0.039
Generator efficiency	0.91	0.84	0.79	0.72	0.67	0.60	0.50
L-T-R conversion efficiency	0.30	0.45	0.51	0.64	0.67	0.73	0.83
Overall harvester efficiency	0.28	0.38	0.40	0.46	0.45	0.44	0.42

presented earlier a factor of 0.62 was applied to the power output to account for the lost linear to rotational motion.

In order to quantify the harvesting efficiency an energy analysis was conducted. The energy loss between the shaker arm and primary shaft (linear to rotational conversion efficiency), generator efficiency and energy loss between the shaker arm to generator (harvesting efficiency). Table 5 displays the efficiencies for various load resistances for 25:1 gear ratio. The results show an optimum load resistance existed that maximized the overall efficiency of the system. At the optimum load resistance of 5,000 Ω the linear to rotational conversion efficiency was 64 % which agrees with the value of 62 % that was empirically determined.

Conclusion

This study presented the design, modeling, fabrication and characterization of a novel energy harvester. By combining a vibration isolator with a vibration absorber relative motion was created without amplification of original source displacement by cancelling the vibration at one location and transferring the source vibration directly to another location. A linear to rotational converter was implemented to convert the high force low linear displacement into high rotational velocity which was used to create the electrical energy utilizing an optimized permanent magnet generator. The energy harvester generated 45 mW @ 0.9 G base acceleration and weighed 462 g. Through analytical modeling it was determined that an optimized prototype could generate 87 mW @ 1 G base acceleration and only weigh 243 g. The analytical parametric analysis indicated an optimal balance between the bandwidth and maximum power harvested. Through simulation it was shown that the critical mass for the system was the absorber mass and that an optimum load resistance exists for each absorber mass. This result suggests that mechanical energy from the vibrating source is harvested, however increasing electrical energy extraction decreases the relative motion created by the vibration isolator and absorber combination. Increasing the absorber mass mitigates this loss in relative motion and therefore increases the power that can be harvested.

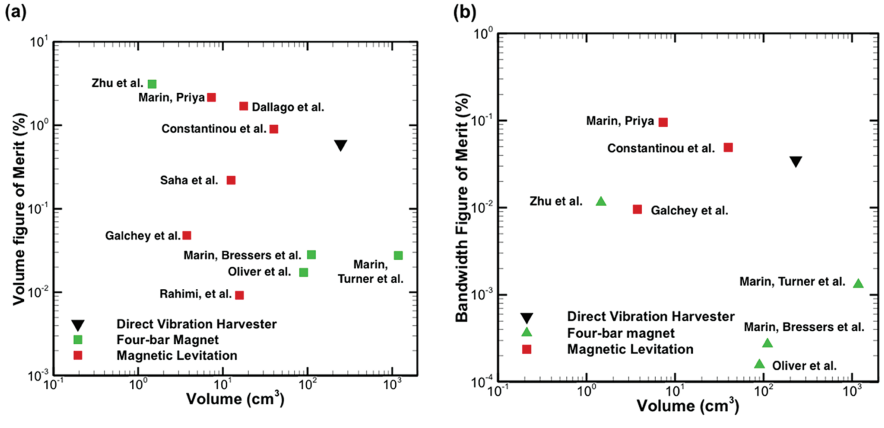

Figure 16: Comparing the direct vibration harvester to the previous state of art for inductive vibration energy harvesters (a) volume figure of merit as a function of volume and (b) bandwidth figure of merit as a function of volume.

Furthermore, increases in absorber mass to levels higher than the primary mass generated higher power normalized by mass values which validates conventional vibration absorber design theory. The reason for the result is still undetermined, but in future work the trend will be confirmed experimentally which should provide further insight on the performance of the isolator and absorber combination.

Figure 16 compares the performance of the direct vibration harvester with the previous state of the art. We can calculate a volume figure of merit F_0M_v and a bandwidth figure of merit F_0M_{BW} (Mitcheson, Yeatman, and Rao 2008) as:

$$F_0M_v = \frac{Useful\ Power\ Output}{\frac{1}{16}Y_0\rho_{AU}Vol^{\frac{4}{3}}\omega^3} \quad [18]$$

$$F_0M_{BW} = F_0M_v \times \frac{BW_{1\,db}}{\omega} \quad [19]$$

where Y_0 is the source displacement, Vol is the total prototype volume, ω is the resonant frequency or center frequency and $BW_{1\,db}$ is the bandwidth 1 dB down from the value at the center frequency. Our multi-degree of freedom direct vibration harvester (DVH) performance was similar to the magnetic levitation prototypes but improved upon the performance of the four-bar magnet prototypes. The mechanisms in this direct vibration harvester are more complicated than all of the other harvesters yet the performance of the initial prototype was still comparable. These results suggest that while there were extra losses in efficiency due to the linear to rotational converter, clutches, and gear train the performance to existing technologies is similar which does not have the extra losses. Based on the simulation the power normalized by mass could increase by 3X by varying the absorber and primary masses.

Acknowledgements: The authors gratefully acknowledge the financial support from Pratt & Whitney.

References

Aldraihem, O., and A. Baz. 2011. "Energy harvester with a dynamic magnifier." *Journal of Intelligent Material Systems and Structures* 22:521–30.

Arafa, M., W. Akl, A. Aladwani, O. Aldraihem, and A. Baz. 2011. "Experimental implementation of a cantilevered piezoelectric energy harvester with a dynamic magnifier." *Proceedings of SPIE 7977*.

Beeby, S. P., M. J. Tudor, and N. M. White. 2006. "Energy harvesting vibration sources for microsystems applications." *Measurement Science and Technology* 17:175.

Bonisoli, E., A. Canova, F. Freschi, S. Moos, M. Repetto, and S. Tornincasa. 2010. "Dynamic simulation of an electromechanical energy scavenging device." *IEEE Transactions on Magnetics* 46:2856–9.

Chtiba, O. M., S. Choura, A. H. Nayfeh, and S. El-Borgi. "Vibration confinement and energy harvesting in flexible structures using collocated absorbers and piezoelectric devices." *Journal of Sound and Vibration* 2010. 329:261–76.

Constantinou, P., P. H. Mellor, and P. Wilcox. 2007. "A model of a magnetically sprung vibration generator for power harvesting applications." IEEE International.

Cornwell, P. J., J. Goethal, J. Kowko, and M. Damianakis. 2005. "Enhancing power harvesting using a tuned auxiliary structure." *Journal of Intelligent Material Systems and Structures* 16:825–34.

Dallago, E., M. Marchesi, and G. Venchi. 2010. "Analytical model of a vibrating electromagnetic harvester considering nonlinear effects." *IEEE Transactions on Power Electronics* 25:1989–97.

El-hami, M., P. Glynne-Jones, N. M. White, M. Hill, S. Beeby, E. James, A. D. Brown, and J. N. Ross. 2001. "Design and fabrication of a new vibration-based electromechanical power generator." *Sensors and Actuators A* 92:335–42.

Galchev, T., K. Hanseup, and K. Najafi. 2011. *Journal of Microelectromechanical Systems* 20:852–66.

Glynne-Jones, P., M. J. Tudor, S. P. Beeby, and N. M. White. 2004. "An electromagnetic, vibration-powered generator for intelligent sensor systems." *Sensors and Actuators A* 110:344–9.

Lee, S., B. D. Youn, and B. C. Jung. 2009. "Robust segment-type energy harvester and its application to a wireless sensor." *Smart Materials and Structures* 18:095021.

Li, W., T. S. Liu, and C. C. Hsiao. 2011. "A miniature generator using piezoelectric bender with elastic base." *Mechatronics* 21:1183–9.

Li, Z., L. Zuo, J. Kuang, and G. Luhrs. 2013. "Energy-harvesting shock absorber with a mechanical motion rectifier." *Smart Materials and Structures* 22:025008.

Ma, P. S., J. E. Kim, and Y. Y. Kim. 2010. "Power-amplifying strategy in vibration-powered energy harvesters." *Proceedings of SPIE* 7643.

Mann, B. P., and N. D. Sims. 2009. *Journal of Sound and Vibration* 319:515–30.

Marin, A., S. Bressers, and S. Priya. 2011. "Multiple cell configuration electromagnetic vibration energy harvester." *Journal of Physics D: Applied Physics* 44:295501.

Marin, A., and S. Priya. 2012. "Multi-mechanism vibration harvester combining inductive and piezoelectric mechanisms." *Proceedings of SPIE* 8341.

Marin, A., Y. Tadesse, A. Bhalla, and S. Priya. 2011. "Multimodal Vibration Harvester Using Inductive and Magnetostrictive Mechanisms." *Integrated Ferroelectrics* 125:111–22.

Marin, A., J. Turner, D. S. Ha, and S. Priya. 2013. "Broadband electromagnetic vibration energy harvesting system for powering wireless sensor nodes." *Smart Materials and Structures* 22:075008.

Mitcheson, P. D., E. M. Yeatman, and G. K. Rao. 2008. "Energy harvesting from human and machine motion for wireless electronic devices." *Proceedings of the IEEE* 96 (9):1457–86.

Oliver, J. M., and S. Priya. 2009. "Design, Fabrication and Modeling of a Four-bar Electromagnetic Vibration Power Generator." *Journal of Intelligent Material Systems and Structures* 21: 1303–16.

O'Donnell, T., C. Saha, S. Beeby, and J. Tudor. 2007. "Scaling effects for electromagnetic vibrational power generators." *Microsystem Technologies* 13:1637–45.

Poulin, G., J. Sarraute, and F. Costa. 2004. "Generation of electrical energy for portable devices: Comparative study of an electromagnetic and a piezoelectric system." *Sensors and Actuators A* 116:461.

Rahimi, A., O. Zorlu, A. Muhtaroglu, and H. Kulah. 2012. "Fully self-powered electromagnetic energy harvesting system with highly efficient dual rail output." *IEEE Sensors Journal* 12 (6):2287–98.

Saha, C. R., T. O'Donnell, N. Wang, and P. McCloskey. 2008. "Electromagnetic generator for harvesting energy from human motion." *Sensors and Actuators A* 147:248–53.

Stephen, N. G. 2006. "On energy harvesting from ambient vibration." *Journal of Sound and Vibration* 293: 409–25.

Tang, X., and L. Zuo. 2011. "Enhanced vibration energy harvesting using dual-mass systems." *Journal of Sound and Vibration* 330:5199–209.

Zhou, W., G. R. Penamalli, and L. Zuo. 2012. "An efficient vibration energy harvester with a multi-mode dynamic magnifier." *Smart Materials and Structures* 21:015014.

Zhu, D., S. Roberts, M. J. Tudor, and S. P. Beeby. 2010. "Design and experimental characterization of a tunable vibration-based electromagnetic micro-generator." *Sensors and Actuators A* 158:284–93.